JACS
JOURNAL OF THE AMERICAN CHEMICAL SOCIETY
Article
pubs.acs.org/JACS

Molecular Motion and Conformational Interconversion of Ir^{I}·COD Included in Rebek's Self-Folding Octaamide Cavitand

Saša Korom,[‡] Eddy Martin,[‡] Stefano A. Serapian,[‡] Carles Bo,[‡] and Pablo Ballester*[,‡,§]

[‡]Institute of Chemical Research of Catalonia (ICIQ), The Barcelona Institute of Science and Technology, Avgda. Països Catalans 16, 43007 Tarragona, Spain

[§]Catalan Institution for Research and Advanced Studies (ICREA), Passeig Lluís Companys 23, 08010 Barcelona, Spain

Supporting Information

ABSTRACT: We report experimental and theoretical evidence of restrained axial rotation for heteroleptic L_2·Ir^{I}·1,5-cyclooctadiene (COD) complexes included in the aromatic cavity of Rebek's self-folding octaamide cavitand. At 298 K, the axial spinning motion of the included organometallic guests was slow on the ^{1}H NMR time scale and produced a proton spectrum for the bound host indicative of C_2 symmetry. Signals corresponding to aromatic protons of the bound host coalesced at 323 K, indicating that the spinning process of the included guest became fast on the ^{1}H NMR time scale and that the complex approached C_4 symmetry. Surprisingly, lowering the temperature of the solution to 193 K induced an additional splitting of the proton signals observed at room temperature for both the bound host and the included guest. We propose the emergence of a new element of chirality in the complexes, which was associated with a slow interconversion, on the ^{1}H NMR time scale between the two chiral twisted-boat conformers of the chelated COD included in the already chiral cavity of the container. This leads to the inclusion complexes existing in solution as pairs of two racemic diastereomers. We estimated that the racemization barrier for the two cyclochiral conformers of the Ir^{I} chelated COD was 5 kcal mol^{-1} higher as an included organometallic complex than as free in solution. Furthermore, we performed a van't Hoff plot and determined that the inclusion of the organometallic complex in the cavitand was endothermic and exclusively driven by entropy (ΔH = 5.9 kcal mol^{-1} and ΔS = 33.9 cal mol^{-1} K^{-1}).

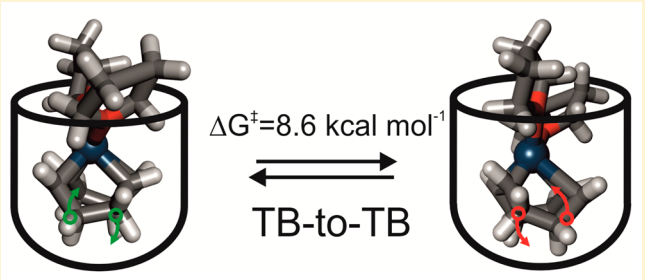

INTRODUCTION

The encapsulation/inclusion of organometallic species within molecular vessels alters their red-ox properties,[1−4] stabilizes reactive intermediates,[5] and mediates their chemical reactivity.[6,7] This latter function can be considered as a synthetic approach to mimic metalloenzyme active sites, and interesting results have been obtained through its implementation.[8−12] Moreover, the confinement of an organometallic catalyst within a molecular cavity tends to increase its stability (TON) and endows substrate selectivity on its chemical reactions.[13,14] Molecular containers might function as second-sphere ligands not covalently bound to the metal center. Unexpected reactivity patterns emerge as a consequence of the intrinsic differences in the catalyst's environment provided by the inner space of the molecular container compared to the bulk solution.[15−17] In this regard, we became interested in investigating the use of deep aromatic cavitands derived from resorcin[4]arenes[18] as molecular containers for catalytic organometallic species with the aim to perform catalytic reactions using the resulting inclusion complexes. As a result of our investigation, we reported the selective catalytic hydrogenation of norbornadiene to norbornene mediated by the inclusion complex of the self-folding octaamide cavitand **1** and rhodium(I) bis-norbornadiene, Rh^{I}·$(NBD)_2$, $\mathbf{2}^+$ (Figure 1).[19] We also described a series of inclusion complexes prepared using pyridyl derivatives of self-folding cavitand **1** as containers of $\mathbf{2}^+$ and showed that these too were able to facilitate the catalytic hydrogenation of norbornadiene.[20]

We hypothesized that inclusion complexes of cavitand **1**[21,22] with organometallic catalytically active species containing other metals than Rh^{I} were also feasible. To this end, in light of the large number of monocationic iridium complexes available, we decided to pursue the inclusion of the iridium(I) bis-(cyclooctadiene) monocationic complex Ir^{I}·$(COD)_2$, $\mathbf{3}^+$, in the deep aromatic cavity of **1** (Figure 1). The organometallic complex $\mathbf{3}^+$ and its counterpart $\mathbf{2}^+$ are monocationic species featuring a relatively similar size and shape. However, the COD ligand is slightly larger than NBD and more conformationally flexible. Molecular modeling studies showed a nice complementarity in size and shape between $\mathbf{3}^+$ and the aromatic cavity of **1**. Here, we describe the results of our studies on the inclusion process of the Ir^{I}·$(COD)_2$ cation in the aromatic cavity of cavitand **1**. Surprisingly, the Ir^{I} metal center was included in the cavity of **1** only when coordinated to a single COD ligand. The resulting inclusion complex, Ir^{I}·COD⊂**1**,

Received: December 3, 2015
Published: January 26, 2016

DOI: 10.1021/jacs.5b12646
J. Am. Chem. Soc. 2016, 138, 2273−2279

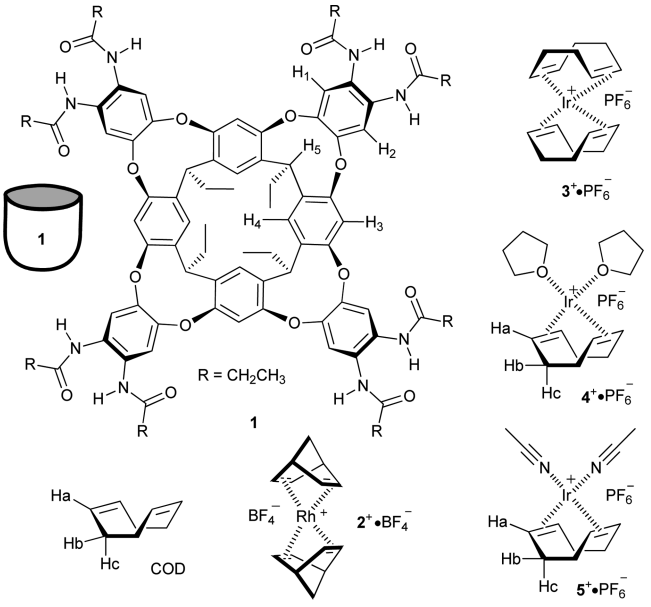

Figure 1. Line drawing structures of self-folding octaamide cavitand **1**; cationic organometallic complexes: $Rh^{I}\cdot(NBD)_2$, $\mathbf{2}^+$; $Ir^{I}\cdot(COD)_2$, $\mathbf{3}^+$; $(THF)_2\cdot Ir^{I}\cdot COD$, $\mathbf{4}^+$; $(CH_3CN)_2\cdot Ir^{I}\cdot COD$, $\mathbf{5}^+$, and ligand: 1,5-cyclooctadiene (COD). The schematic representation of **1** as a hollow cup is also shown.

displayed a rotational motion of the included organometallic species that was slow on the ^{1}H NMR time scale even at room temperature. At low temperatures, the interconversion process between the chiral twisted-boat (TB) conformations of the coordinated COD ligand in the complex $Ir^{I}\cdot COD\subset\mathbf{1}$ also became slow on the proton chemical shift time scale. This unexpected result allowed us to set a limit of at least 4 kcal mol^{-1} for the increase in the energy barrier of the TB−TB conformational interconversion occurring in the confined space of **1** with respect to the same process in $Ir^{I}\cdot(COD)_2$ or free COD in the bulk solution. The unidirectional orientation of the amide groups in **1** was kinetically stable on the proton chemical shift time scale and rendered the cavitand a chiral host. In addition, at low temperatures (183 K) the chiral TB conformation of the COD was also kinetically stable. Thus, the resulting $Ir^{I}\cdot COD\subset\mathbf{1}$ complexes existed in solution as pairs of racemic diastereoisomers that were found to be isoenergetic.

RESULTS AND DISCUSSION

Compounds **1**, **3**, and **5** were synthesized according to published procedures (Figure 1).[22−24] At room temperature, the ^{1}H NMR spectrum of the octaamide cavitand **1** in THF-d_8 solution showed a broad singlet for the amide NH hydrogen atoms (δ= 9.7 ppm) that was consistent with C_{4v} symmetry (Figure 2a). This observation was indicative of a fast interconversion on the ^{1}H NMR time scale between the two cycloenantiomers of **1** (*P* and *M*).[21,22] Variable-temperature ^{1}H NMR experiments assigned an energy barrier of 13 kcal mol^{-1} to the interconversion process at the coalescence temperature of 273 K (see SI). At room temperature, the methine protons (H_5) of **1** resonated at δ = 5.7 ppm, indicating that the cavitand **1** was in the vase conformation (Figure 2a).[25,26,21,22]

The addition of ∼0.8 equiv of the organometallic complex $Ir^{I}\cdot(COD)_2$, $\mathbf{3}^+$, to a 4.00 mM THF-d_8 solution of cavitand **1** induced the observation of separate proton signals for free and bound host (Figure 2b). In addition, the amide NHs of the

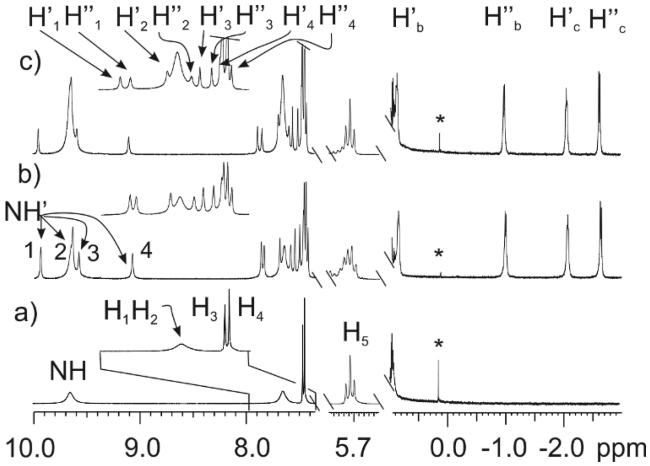

Figure 2. Selected regions of the ^{1}H NMR spectra (400 MHz, 298 K of, THF-d_8) of: (a) [**1**] = 4.00 mM); (b) a mixture of [**1**] = 4 mM and [$\mathbf{3}^+$] = 3.27 mM; and (c) a mixture [**1**] = 4.00 mM and [$\mathbf{5}^+$] = 3.27 mM). See Figure 1 for proton assignments. Primed and second primed letters indicate protons in bound host and bound guest. The insets in the panels are expansions of the 7.5−8.0 ppm region, and * denotes grease.

bound host resonated as four separate signals (Figure 2b, NH′ 1−4). A signal at ≈5.7 ppm for the methine protons of the bound **1** supported the adoption of a vase conformation. We also observed the emergence of a new set of four highly upfield shifted proton signals (designated as H_b', H_b'', H_c', and H_c'' in Figure 2b,c) that were assigned to COD protons of the included organometallic complex in the aromatic cavity of **1**. It is worth noting that signals corresponding to the protons of free COD (δ = 5.5 (H_a), 2.3 (H_b), 1.7 (H_c) ppm) were also detected in the ^{1}H NMR spectrum of the mixture. However, the exact amount of free COD in solution was difficult to determine due to overlap with other proton signals from the host. The highly upfield shifted signals for the metal coordinated COD included in **1** indicated that the ligand was close to the tapered end of the container. The observed resonances for free COD suggested that the included Ir^{I} complex possessed a single COD ligand. This latter hypothesis was validated by performing a titration experiment using the heteroleptic $(CH_3CN)_2\cdot Ir^{I}\cdot COD$ complex, $\mathbf{5}^+$ (Figure 1). The ^{1}H NMR spectrum of the resulting inclusion complex $\mathbf{5}^+\subset\mathbf{1}$ was superimposable with that obtained with $Ir^{I}\cdot(COD)_2$, $\mathbf{3}^+$, and **1** (Figure 2c). This result provided evidence that cavitand **1** formed the caviplex $Ir^{I}\cdot COD\subset\mathbf{1}$ in the presence of the organometallic complex $\mathbf{3}^+$, where one of the COD ligands was dissociated.

It is important to note that the organometallic complex $\mathbf{3}^+$ dissolved in THF-d_8 shows partial dissociation (≈ 15%) of one of the COD ligands in the absence of host **1**. This observation implies the formation of a heteroleptic complex, most likely resulting from one COD ligand being replaced by two solvent molecules affording the putative $(THF\text{-}d_8)_2\cdot Ir^{I}\cdot COD$, $\mathbf{4}^+$ complex (Figure 1). Such COD ligand dissociation was not observed when methylene chloride-d_2 was used as a solvent.[27] The acetonitrile ligands in the complex $\mathbf{5}^+$ did not exchange with solvent molecules (THF-d_8). These observations allowed us to hypothesize that the formation of the $\mathbf{4}^+\subset\mathbf{1}$ complex did not entail the inclusion of the homoleptic $Ir^{I}\cdot(COD)_2$ complex $\mathbf{3}^+$ followed by dissociation of one of the COD ligands, but rather the direct inclusion of the heteroleptic $(THF\text{-}d_8)_2\cdot Ir^{I}\cdot$

DOI: 10.1021/jacs.5b12646
J. Am. Chem. Soc. 2016, 138, 2273−2279

COD complex 4^+ present in low concentration in solution. Moreover, the addition of incremental amounts of COD to a solution containing the $4^+\subset\mathbf{1}$ caviplex led to a decrease in intensity of the proton signals for the $4^+\subset\mathbf{1}$ complex and to an increase in the intensities of the proton signals assigned to free **1** and 3^+. The proposed binding process is shown in Figure 3.

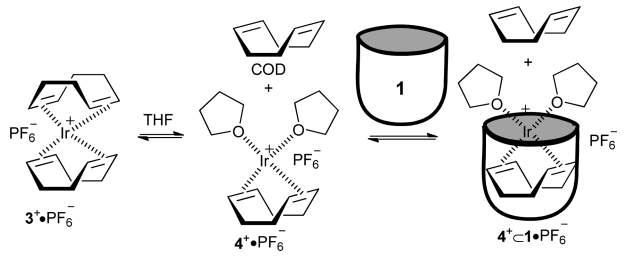

Figure 3. Binding equilibria involved in the inclusion of Ir^I·COD by cavitand **1** using the organometallic complex 3^+ as metal precursor.

The observation of four amide NH protons signals for bound **1** in the ^{1}H NMR spectrum of the encapsulation complexes $4^+\subset\mathbf{1}$ and $5^+\subset\mathbf{1}$ was completely unexpected. Previously studied encapsulation complexes of octaamide **1** with other organometallic species (i.e., 2^+) showed only two amide NH proton signals for bound **1**. This is the expected result of a slow interconversion process on the proton chemical shift time scale between the two cycloenantiomers of host **1**, *M* and *P*, upon guest encapsulation. It is well established that the element of asymmetry in bound **1** results from the unidirectional orientation of its eight hydrogen-bonded amide groups that are kinetically stable on the chemical shift time scale. This arrangement of amide groups stabilized the vase conformation of **1** as a mixture of two cycloenantiomers displaying C_4 symmetry in solution.[19,28]

The unique pattern of four different NH signals observed for the $4^+\subset\mathbf{1}$ and $5^+\subset\mathbf{1}$ complexes displayed an integration ratio of 2:2:2:2.[29] This observation can be explained by slow axial rotational motion (spinning) of the included guest on the ^{1}H NMR time scale. This would reduce the symmetry of the bound host from C_4 to C_2 and, as depicted in Figure 4, render the aromatic protons of bridging adjacent walls chemically nonequivalent (H_1', H_1'' and H_2', H_2'').

In agreement with the slow cycloenantiomerization of the host and the slow axial rotation of the guest, we also observed eight different signals for the aromatic protons of the bound host **1** in the $4^+\subset\mathbf{1}$ complex (see Figures 2b and 4 for proton assignments).

The reasons for the slow axial rotation of the included Ir^I·COD in host **1** are not clear to us. There are no apparent steric clashes between the guest and the host that could slow down the spinning process. We expected the existence of attractive forces (cation−π and CH−π interactions) between the electron-rich inner surface of the cavitand and the outer electron-poor surface of the cationic organometallic complex. Most likely, as the guest rotates around the host's axial axis, some CH−π interactions are weakened, and the energy of the complex increases to a transition state where the guest is rotated close to 67.5° from the starting point. This transition state is preceded by a high-energy intermediate in which the guest is rotated close to 45° from the starting point. Further guest rotation, past the transition state, leads to the next degenerate energy minimum found at 90° from the starting point (*vide infra*).

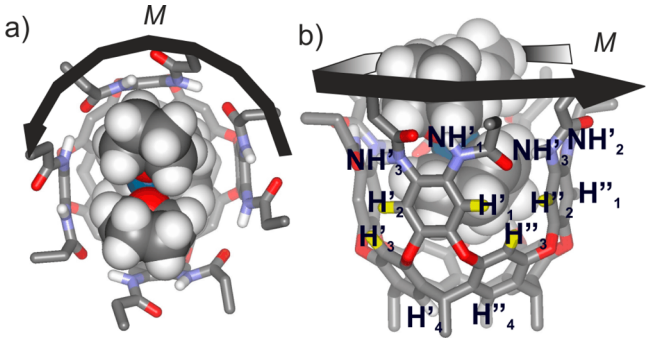

Figure 4. MM3 energy-minimized structure of the *M* enantiomer of the inclusion complex $4^+\subset\mathbf{1}$: (a) top and (b) side views. The shown unidirectional orientation of the hydrogen-bonded amide groups constitutes the source of the supramolecular element of asymmetry of the complex. Selected NH and aromatic protons are assigned. The majority of nonpolar hydrogen atoms are omitted for clarity. 4^+ is shown as CPK model and **1** in stick representation. The double bonds of the COD face the lateral dioxo-phenyl walls, while the methylene groups are near the walls in the front and the back. The magnetic environment provided by the aromatic walls is different due to the slow spinning of 4^+. The ethyl chain in the lower rim is shown as a methyl group for clarity.

The counterclockwise spinning process of the cationic guest in the $4^+\subset\mathbf{1}$ complex was studied *in silico* at the DFT level of theory using the Gaussian09 software package.[30] The chosen density functional was PBE,[31] with the crucial addition of D3[32] dispersion corrections for a more accurate treatment of CH−π interactions. Ir^I electrons were simulated using the LANL2DZ effective core potential and basis set,[33] whereas electrons on remaining atoms were all treated with a 6-311G(d,p) basis set. The challenging search of a transition state (with one imaginary vibrational mode, see SI) for the spinning process led to the identification of a structure that was 6.65 kcal mol^{-1} higher in energy than the optimized and degenerate energy structures of the $4^+\subset\mathbf{1}$ complex at 0° (Figure 4) and 90° rotation of the included guest.

The theoretically calculated barrier for the spinning process corresponds to a rate constant of $k_r > 8 \times 10^7$ s^{-1} at 298 K, which certainly does not agree with a process displaying slow chemical exchange on the ^{1}H NMR scale ($k_r < 400$ s^{-1} for two peaks separated by 200 Hz). We suspect that the "friction" caused by the spinning process of included 4^+ with solvent molecules in its second or third coordination spheres might constitute an important factor, although difficult to model, for increasing the calculated energy barrier of the spinning process to values more consistent with experiment.

A 2D EXSY experiment performed on the $5^+\subset\mathbf{1}$ complex showed cross peaks due to chemical exchange between amide NH signals. This result indicated that, although the spinning of the guest and cycloenantiomerization of the host were slow on the ^{1}H NMR time scale, they were fast on the EXSY time scale. Unfortunately, the overlap of cross-peaks due to both chemical exchange processes prohibited the determination of their corresponding energy barriers.

The 2D EXSY experiment (see SI) showed a nice, clean pattern of cross peaks between the upfield shifted protons of included 5^+ (H_b'/H_b'' and H_c'/H_c'') and revealed the existence of a third pair of protons for the included guest (designated as H_a'/H_a''). This latter pair was buried under the intense proton signals of the host's ethyl groups. To understand the splitting pattern observed for the protons of the included Ir^I·COD

DOI: 10.1021/jacs.5b12646
J. Am. Chem. Soc. 2016, 138, 2273−2279

(three pairs for a total of six separate signals), one must consider the conformational features displayed by free and metal-coordinated COD. Experimental and theoretical studies support the TB conformation of COD as the lowest energy structure.[34−37] The TB conformation of COD has C_2 symmetry and constitutes an example of a conformationally chiral molecule.[38,39] Therefore, there are two possible TB enantiomeric conformers of COD. To assign the absolute configuration to each conformer, we applied rules of axial chirality, looking at the face of the TB conformer of COD defined by the single bond connecting two methylene groups. The sense of the torsion needed to superimpose the single bond in front with that in back defined the absolute *P* or *M* configuration of each conformer (Figure 5).

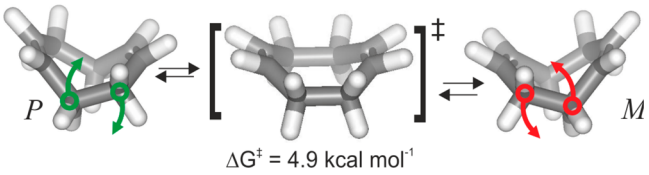

Figure 5. Interconversion equilibrium between the two enantiomeric TB conformers of COD via the B conformer.

A TB-to-TB interconversion of free COD in solution proceeding via a boat (B) transition state (Figure 5) has been offered as an explanation for the coalescence process observed in the ^{1}H NMR spectrum of the ligand at 105 K (ΔG = 4.9 kcal mol^{-1}).[36] Thus, at room temperature, COD and metal-chelated COD in complexes like **3**$^+$ or **5**$^+$ showed a fast interconversion on the ^{1}H NMR time scale between the two TB conformers, and only three different proton signals (vinyl, axial and equatorial methylene protons) are typically observed in their spectra. While this result is consistent with the C_{2v} symmetry exhibited by the B conformer, it is in fact due to the fast TB-to-TB interconversion. We are not aware of any study performed on mono- or bis-COD Ir^I complexes addressing the analogous interconversion process between the TB conformers of the metal-coordinated ligand. Our own DFT calculations on free **4**$^+$ (see SI) indicate that the interconversion barrier is in the range of 3.5 kcal mol^{-1}. In addition, most publications depict the line drawing structure of COD in the B conformation (Figure 6). However, a search in the Cambridge Crystallographic Data Centre (CCDC) rapidly identified X-ray crystal structures of Ir^I COD complexes showing the existence of metal-chelated ligand in TB conformation in the solid state.[40] Molecular modeling studies (MM3 as implemented in SCIGRESS v3.0) also showed that the energy minimized structure of the **4**$^+$⊂**1** complex displayed the COD ligand in the TB conformation.

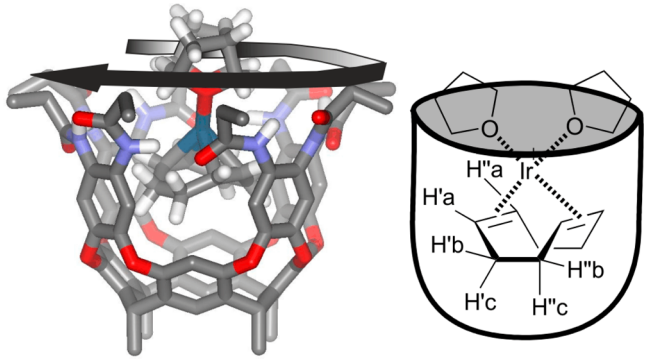

Figure 6. (Left) Stick representation of the MM3 energy-minimized structure of the *P*-cyclochiral enantiomer of **1** including the organometallic complex **4**$^+$ displaying the COD ligand locked in B conformation. (Right) Schematic representation of the chiral complex **4**$^+$⊂*P*-**1** with proton assignments for the included COD.

Based on the discussion above, we surmised that the TB-to-TB interconversion for the metal-chelated COD in the included **4**$^+$ or **5**$^+$ organometallic complexes was also fast on the chemical shift time scale (*vide infra*). For this reason, the appearance at room temperature of six different COD proton signals in the ^{1}H NMR spectra of the inclusion complexes **4**$^+$⊂**1** and **5**$^+$⊂**1** (Figure 2b,c, upfield regions) was rationalized as a consequence of the chiral nature of the container **1**. Upon complexation in chiral host **1**, the protons of the COD in the included guests became diastereotopic (two different vinylic protons and two distinct pairs of equatorially and axially oriented protons), reducing the guest symmetry from C_{2v}-like to C_2, independent of the spinning rate.

The cross peaks of the chemical exchange processes observed in the EXSY experiments for the proton signals of included **4**$^+$ and **5**$^+$ were produced by the slow interconversion on the proton chemical shift time scale between the two cycloenantiomers of the bound container **1**. From the integral values of the diagonal and cross peaks of the diastereotopic protons of included **5**$^+$, we determined, based on a two site exchange model, an energy barrier of 16.5 kcal mol^{-1} for the cycloenantiomerization process of the container. On the other hand, using the data of a 2D-EXSY experiment performed on a solution of **1** containing a large excess of the **5**$^+$ (10 equiv; see SI) and based on a three sites exchanges model, we calculated at room temperature the energy barrier for the release of the organometallic guest and the energy barrier for the host's cycloenantiomerization. These were found to be 18.0 and 16.8 kcal mol^{-1}, respectively, as depicted in Figure 7. The observation of a slow in−out exchange process for **5**$^+$ is surprising given the open end of the container and the low stability constant value estimated for the complex, K_a(**5**$^+$⊂**1**) < 1000 M^{-1}. However, as reported by Rebek et al.[21,22] the exchange dynamics of inclusion complexes involving **1** are controlled by the mechanism of guest exchange and not by the thermodynamic stability of the complex. The lowest energy pathway for the in−out guest exchange requires the bound host to change its conformation from vase to kite. This conformational change is associated with a significant energetic penalty of 10−12 kcal mol^{-1} for cavitands with bridging aromatic walls that are not hydrogen bonded.[41] In the specific case of **1**, the cost of the disruption of hydrogen bonds must be added, thus increasing the energy barrier of the in−out exchange to 18.0 kcal mol^{-1}.

The 2 kcal mol^{-1} difference that was consistently found between the barriers for cycloenantiomerization and in−out guest's exchange processes suggested that the unfolding of the vase required the breaking of the intramolecular hydrogen bonds and the host−guest interactions. More importantly, because the two processes featured different energy barriers we concluded that they are not coupled.[42] Cycloenantiomerization of **1** might occur without guest exchange.

Variable-temperature ^{1}H NMR experiments performed on solutions containing either the complex **4**$^+$⊂**1** or **5**$^+$⊂**1** showed coalescence of the signals for the H$_1$′ and H$_1$″ protons at 323 K (Figure 8). This result indicated that the spinning of the

DOI: 10.1021/jacs.5b12646
J. Am. Chem. Soc. 2016, 138, 2273−2279

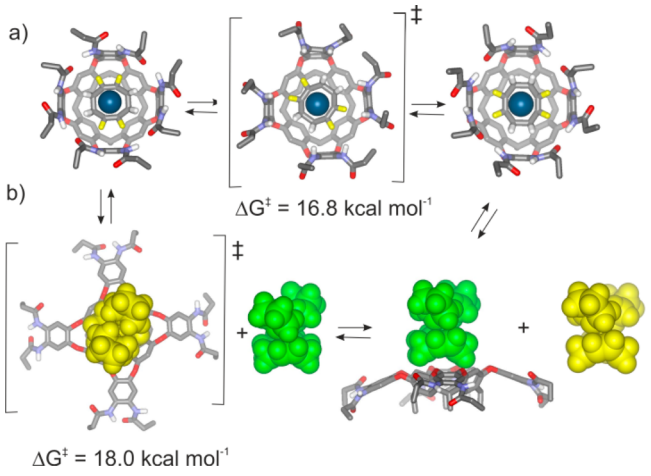

Figure 7. Proposed sequences for (a) the spinning process of the included organometallic complex, possibly coupled to the cycloenantiomerization of the host, and (b) the in−out exchange of the organometallic guest coupled with host cycloenantiomerization. In panel (a) the THF molecules are omitted for clarity, and the complexes are seen from the top. Hydrogen atoms of the double bonds of the COD are colored in yellow, and the Ir^{I} metal is shown in dark cyan CPK. From left to right, the guest $\mathbf{4}^{+}$ is rotated 0°, 45°, and 90° counterclockwise. In panel (b) the organometallic guest $\mathbf{4}^{+}$ is shown as CPK model (bound: yellow, free: green) before the exchange. Putative structures for the transition states with the determined values for the energy barriers are also indicated.

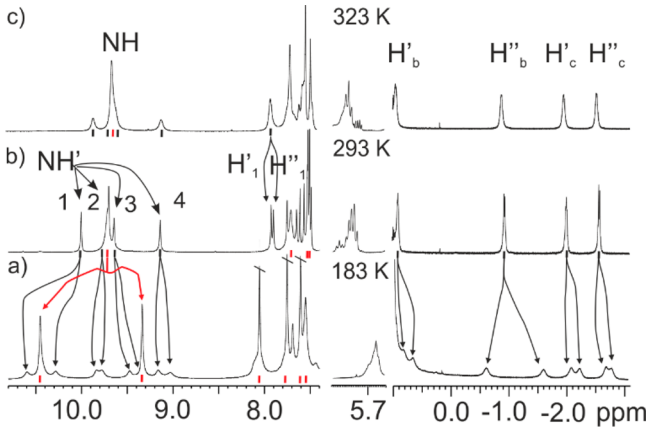

Figure 8. Selected regions of variable-temperature ^{1}H NMR experiments of a THF-d_8 solution containing [**1**] = 4.00 mM and [$\mathbf{3}^{+}$] = 3.27 mM at: (a) 183, (b) 298, and (c) 323 K. The splitting of the proton signals for the bound host and the bound guest at 183 K is indicated with black arrows. Red arrows show the splitting of the NHs of the free host at this temperature. The coalescence of H'_1 and H''_1 protons of the bound host at 323 K is also indicated. Red tick marks indicate protons in the free host and black marks in the complex. See text for additional details.

included organometallic complex became fast for these proton signals and allowed the calculation of an energy barrier of 16.6 kcal mol^{-1} (k_{exch} = 2.22 ($\Delta\nu$) = 36 s^{-1}) at 323 K. The coincidence in energy barriers for guest's spinning and host's cycloenantiomerization processes suggested that these processes might indeed be coupled.

Finally, lowering the temperature to 183 K (Figure 8a) induced the splitting of most of the proton signals in bound **1** and in included $\mathbf{4}^{+}$ or $\mathbf{5}^{+}$ in two sets of equal intensity. A likely explanation can be found with the existence of slow exchange on the ^{1}H NMR time scale between the two chiral TB conformations of COD ligand in the included Ir^{I}·COD. The fact that the TB conformation of the included Ir^{I}·COD became kinetically stable on the NMR time scale added an additional element of asymmetry (conformational chirality) to that provided by the unidirectional orientation of amide groups in the inclusion complexes $\mathbf{4}^{+}\subset\mathbf{1}$ and $\mathbf{5}^{+}\subset\mathbf{1}$. In short, at 193 K and below, the $\mathbf{4}^{+}\subset\mathbf{1}$ and $\mathbf{5}^{+}\subset\mathbf{1}$ complexes are present in solution as a pair of racemic diastereoisomers (Figure 9).[43]

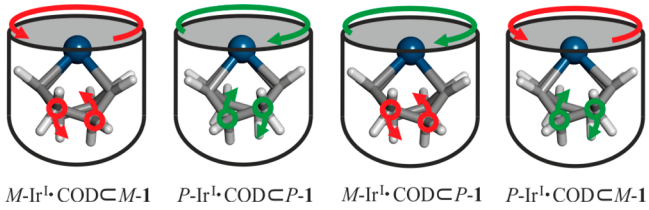

Figure 9. Schematic representations of the four diastereoisomeric complexes of $\mathbf{4}^{+}\subset\mathbf{1}$. The absolute configurations assigned to the senses of rotation of the amide groups at the upper rim of **1** and the TB conformer of the COD in the included organometallic complex $\mathbf{4}^{+}$ are depicted with colored arrows. THF ligands are omitted for clarity.

The equal intensity exhibited by the proton signals corresponding to the two diastereoisomers, i.e., *P*-$\mathbf{4}^{+}\subset$*P*-**1** and *M*-$\mathbf{4}^{+}\subset$*P*-**1**, testified to the complete lack of chiral recognition in the inclusion of the two enantiomers of $\mathbf{4}^{+}$ in the chiral cavity of **1**.

Using the coalescence temperature method, we calculated an energy barrier of $\Delta G^{\ddagger}$ = 8.6 kcal mol^{-1} for the TB-to-TB conformational exchange of the Ir^{I}·COD included in **1**. This value corresponds to an increase of almost 4 kcal mol^{-1} with respect to the barrier of the same process determined experimentally for free COD in solution[36] and of more than 5 kcal mol^{-1} in relation to the theoretically calculated barrier for $\mathbf{4}^{+}$ in the gas phase (see SI). We suggest that a reduction of attractive CH−π interactions occurs upon moving from the TB ground state to the B transition state. Another explanation is that the transition state could be a worse fit for the cavity of **1** and responsible for the significantly larger energy barrier measured for the TB-to-TB conformational exchange for Ir^{I}·COD included in **1**.

Finally, by integration of the separated proton signals of free and bound host and guest, we determined the stability constant values for the $\mathbf{5}^{+}\subset\mathbf{1}$ complex at different temperatures. Surprisingly, the binding constant value diminished as the temperature was lowered $K_a(\mathbf{5}^{+}\subset\mathbf{1}, 274\ \text{K})$ = 620 ± 200 M^{-1} and $K_a(\mathbf{5}^{+}\subset\mathbf{1}, 233\ \text{K})$ = 95 ± 30 M^{-1}. We performed a van't Hoff plot to determine the thermodynamic constants of the binding process (see SI). The linear fit to the experimental data was good and returned the values of ΔH = 5.9 kcal mol^{-1} and ΔS = 33.9 cal mol^{-1} K^{-1}, corresponding to a ΔG of −4.2 kcal mol^{-1} at 298 K. Our findings indicate that the formation of the $\mathbf{5}^{+}\subset\mathbf{1}$ caviplex is endothermic and driven exclusively by entropy. Again, this was not an expected result. THF is a polar organic solvent, and consequently the solvation/desolvation processes that occur upon guest binding seem to play a key role in the thermodynamic stabilization of the complex.[44,45] The methine proton of **1** remained centered at δ = 5.7 ppm throughout the range of studied temperatures, indicating that the host maintained its vase conformation. At high temperatures the Ir^{I} complexes are preferentially solvated by the

DOI: 10.1021/jacs.5b12646
J. Am. Chem. Soc. 2016, 138, 2273−2279

aromatic walls of **1** mainly due to the entropic gain derived from the release of an undefined number of solvent molecules to the bulk.

CONCLUSIONS

We have studied the inclusion process of the monocationic organometallic iridium(I) bicyclooctadiene complex, $\mathbf{3}^+$, into the aromatic cavity of the self-folding octaamide cavitand **1** in THF solution. When dissolved in THF, the organometallic complex $\mathbf{3}^+$ partially dissociated (15%) into a heteroleptic Ir^I complex $\mathbf{4}^+$ that contained a single chelated COD ligand and possibly two monocoordinated THF molecules. At mM concentration, the heteroleptic Ir^I complex $\mathbf{4}^+$ was selectively included in the deep aromatic cavity of cavitand **1** yielding the inclusion complex $\mathbf{4}^+\subset\mathbf{1}$. Using the organometallic complex $(CH_3CN)_2{\cdot}Ir^I{\cdot}COD$, $\mathbf{5}^+$, as guest, an analogous inclusion complex $\mathbf{5}^+\subset\mathbf{1}$ was obtained.[46] The proton signals of the two inclusion complexes were totally superimposable and confirmed the inclusion of the cationic species $Ir^I{\cdot}COD$ in **1**. The included $Ir^I{\cdot}COD$ displayed a spinning motion when included in **1**. At room temperature the spinning rate was slow on the ^1H NMR time scale. This slow rotation produced splitting of the proton signals of the bound cavitand **1**. In addition, the unidirectional orientation of the upper rim amide groups in the bound cavitand **1** was kinetically stable on the chemical shift time scale. This provided an element of asymmetry to the inclusion complexes $\mathbf{4}^+\subset\mathbf{1}$ and $\mathbf{5}^+\subset\mathbf{1}$ that exist in solution as a mixture of two cycloenantiomers. Consequently, the proton signals of the included guest resonated as diastereotopic protons. From the results obtained in variable-temperature ^1H NMR experiments and 2D-EXSY experiments, we determined the energy barriers for the spinning motion of the guest ($\Delta G^{\ddagger}$ = 16.6 kcal mol^{-1}), the cycloenantiomerization of the host ($\Delta G^{\ddagger}$ = 16.8 kcal mol^{-1}), and the in−out exchange of the guest ($\Delta G^{\ddagger}$ = 18.0 kcal mol^{-1}). We propose that the guest spinning motion might be coupled with the host cycloenantiomerization. We suggest that the in−out exchange of the guest followed a different sequence of events that required a change in the conformation of the host from the vase to the kite conformation with the concomitant disruption of most of the intermolecular interactions that stabilized the complexes. At low temperatures, the ^1H NMR signals of the inclusion complexes split in two sets of signals of equal intensity. This observation indicated the existence of a new element of asymmetry, which we assigned to a slow interconversion on the chemical shift time scale between the two TB chiral conformers of the included $Ir^I{\cdot}COD$. We also determined that compared to the organometallic complex free in solution, the energy barrier for the TB-to-TB interconversion of COD is raised by 6 kcal mol^{-1} when the $Ir^I{\cdot}COD$ species is included in **1**. Finally, the thermodynamic constants calculated for the inclusion process of $\mathbf{5}^+$ in the aromatic cavity of **1** indicated that the binding was endothermic and entropically driven.

ASSOCIATED CONTENT

Supporting Information

The Supporting Information is available free of charge on the ACS Publications website at DOI: 10.1021/jacs.5b12646. A dataset collection is available at http://dx.doi.org/10.19061/iochem-bd-1-2.

^1H NMR spectra of 1D variable-temperature experiments, 2D EXSY-NOESY and HSQC spectra, ^1H NMR spectra for the titration of **1** with $\mathbf{3}^+$, data used in the van't Hoff plot, details of the computational study and the obtained results (PDF)

AUTHOR INFORMATION

Corresponding Author

*pballester@iciq.es

Notes

The authors declare no competing financial interest.

ACKNOWLEDGMENTS

The authors thank Gobierno de España MINECO (projects CTQ2014-56295-R, CTQ2014-52824-R, and Severo Ochoa Excellence Accreditation 2014-2018 SEV-2013-0319), Feder funds (CTQ2014-56295-R), and the ICIQ Foundation for funding. S.A.S. thanks the Marie Curie/COFUND scheme ref. 291787-ICIQ-IPMP for funding. We also thank Professors Shannon M. Biros, Grand Valley State University, Allendale, Michigan (U.S.A.) and Louis Adriaenssens, University of Lincoln, Brayford Pool, Lincoln (U.K.) for carefully editing this manuscript.

REFERENCES

(1) Cardona, C. M.; Mendoza, S.; Kaifer, A. E. *Chem. Soc. Rev.* **2000**, *29*, 37−42.
(2) Podkoscielny, D.; Hooley, R. J.; Rebek, J.; Kaifer, A. E. *Org. Lett.* **2008**, *10*, 2865−2868.
(3) Gadde, S.; Batchelor, E. K.; Kaifer, A. E. *Aust. J. Chem.* **2010**, *63*, 184−194.
(4) Sun, W. Y.; Kusukawa, T.; Fujita, M. *J. Am. Chem. Soc.* **2002**, *124*, 11570−11571.
(5) Fiedler, D.; Bergman, R. G.; Raymond, K. N. *Angew. Chem., Int. Ed.* **2006**, *45*, 745−748.
(6) Fiedler, D.; Leung, D. H.; Bergman, R. G.; Raymond, K. N. *Acc. Chem. Res.* **2005**, *38*, 349−358.
(7) Kleij, A. W.; Reek, J. N. H. *Chem. - Eur. J.* **2006**, *12*, 4218−4227.
(8) Slagt, V. F.; Kamer, P. C. J.; van Leeuwen, P. W. N. M.; Reek, J. N. H. *J. Am. Chem. Soc.* **2004**, *126*, 1526−1536.
(9) Slagt, V. F.; Reek, J. N. H.; Kamer, P. C. J.; van Leeuwen, P. W. N. M. *Angew. Chem., Int. Ed.* **2001**, *40*, 4271−4274.
(10) Kuil, M.; Soltner, T.; van Leeuwen, P.; Reek, J. N. H. *J. Am. Chem. Soc.* **2006**, *128*, 11344−11345.
(11) Koblenz, T. S.; Wassenaar, J.; Reek, J. N. H. *Chem. Soc. Rev.* **2008**, *37*, 247−262.
(12) Leenders, S. H. A. M.; Gramage-Doria, R.; de Bruin, B.; Reek, J. N. H. *Chem. Soc. Rev.* **2015**, *44*, 433−448.
(13) Lee, S. J.; Cho, S. H.; Mulfort, K. L.; Tiede, D. M.; Hupp, J. T.; Nguyen, S. T. *J. Am. Chem. Soc.* **2008**, *130*, 16828−16829.
(14) Merlau, M. L.; Mejia, M. D. P.; Nguyen, S. T.; Hupp, J. T. *Angew. Chem., Int. Ed.* **2001**, *40*, 4239−4242.
(15) Leung, D. H.; Bergman, R. G.; Raymond, K. N. *J. Am. Chem. Soc.* **2007**, *129*, 2746−27477.
(16) Leung, D. H.; Bergman, R. G.; Raymond, K. N. *J. Am. Chem. Soc.* **2006**, *128*, 9781−9797.
(17) Brown, C. J.; Toste, F. D.; Bergman, R. G.; Raymond, K. N. *Chem. Rev.* **2015**, *115*, 3012−3035.
(18) Rudkevich, D. M.; Rebek, J. *Eur. J. Org. Chem.* **1999**, *1999*, 1991−2005.
(19) Sarmentero, M. A.; Fernández-Pérez, H.; Zuidema, E.; Bo, C.; Vidal-Ferran, A.; Ballester, P. *Angew. Chem., Int. Ed.* **2010**, *49*, 7489−7492.
(20) Korom, S.; Ballester, P. *Eur. J. Org. Chem.* **2014**, *2014*, 4276−4282.
(21) Rudkevich, D. M.; Hilmersson, G.; Rebek, J. *J. Am. Chem. Soc.* **1997**, *119*, 9911−9912.

DOI: 10.1021/jacs.5b12646
J. Am. Chem. Soc. 2016, 138, 2273−2279

(22) Rudkevich, D. M.; Hilmersson, G.; Rebek, J. *J. Am. Chem. Soc.* **1998**, *120*, 12216−12225.
(23) Dervisi, A.; Carcedo, C.; Ooi, L.-l. *Adv. Synth. Catal.* **2006**, *348*, 175−183.
(24) Day, V. W.; Klemperer, W. G.; Main, D. J. *Inorg. Chem.* **1990**, *29*, 2345−2355.
(25) Moran, J. R.; Ericson, J. L.; Dalcanale, E.; Bryant, J. A.; Knobler, C. B.; Cram, D. J. *J. Am. Chem. Soc.* **1991**, *113*, 5707−5714.
(26) Cram, D. J.; Choi, H. J.; Bryant, J. A.; Knobler, C. B. *J. Am. Chem. Soc.* **1992**, *114*, 7748−7765.
(27) DCM was not used as solvent in the binding studies because it strongly competed with guest binding.
(28) Zuidema, E.; Sarmentero, M. A.; Bo, C.; Ballester, P. *Chem. - Eur. J.* **2008**, *14*, 7285−7295.
(29) Theoretical predictions using DFT calculations at the PBE level of theory (LANL2DZ effective core potential basis set for Ir; 6-311G(d,p) basis set for the remaining atoms) confirmed TB conformation of the guest $(CH_3\text{-}O\text{-}CH_3)_2{\cdot}Ir^{I}{\cdot}COD$ included within cavitand **1** (with methyl groups instead of ethyl). Chemical shifts calculated for COD and NH protons on this structure (GIAO method) are in qualitative agreement with experimentally determined values.
(30) Frisch, M. J.; Trucks, G. W.; Schlegel, H. B.; Scuseria, G. E.; Robb, M. A.; Cheeseman, J. R.; Scalmani, G.; Barone, V.; Mennucci, B.; Petersson, G. A.; Nakatsuji, H.; Caricato, M.; Li, X.; Hratchian, H. P.; Izmaylov, A. F.; Bloino, J.; Zheng, G.; Sonnenberg, J. L.; Hada, M.; Ehara, M.; Toyota, K.; Fukuda, R.; Hasegawa, J.; Ishida, M.; Nakajima, T.; Honda, Y.; Kitao, O.; Nakai, H.; Vreven, T.; Montgomery, J. A., Jr.; Peralta, J. E.; Ogliaro, F.; Bearpark, M.; Heyd, J. J.; Brothers, E.; Kudin, K. N.; Staroverov, V. N.; Kobayashi, R.; Normand, J.; Raghavachari, K.; Rendell, A.; Burant, J. C.; Iyengar, S. S.; Tomasi, J.; Cossi, M.; Rega, N.; Millam, J. M.; Klene, M.; Knox, J. E.; Cross, J. B.; Bakken, V.; Adamo, C.; Jaramillo, J.; Gomperts, R.; Stratmann, R. E.; Yazyev, O.; Austin, A. J.; Cammi, R.; Pomelli, C.; Ochterski, J. W.; Martin, R. L.; Morokuma, K.; Zakrzewski, V. G.; Voth, G. A.; Salvador, P.; Dannenberg, J. J.; Dapprich, S.; Daniels, A. D.; Ö. Farkas, Foresman, J. B.; Ortiz, J. V.; Cioslowski, J.; Fox, D. J. *Gaussian 09*, Revision D.01; Gaussian, Inc., Wallingford, CT, 2009.
(31) Perdew, J. P.; Burke, K.; Ernzerhof, M. *Phys. Rev. Lett.* **1996**, *77*, 3865−3868.
(32) Grimme, S.; Antony, J.; Ehrlich, S.; Krieg, H. *J. Chem. Phys.* **2010**, *132*, 154104.
(33) Hay, P. J.; Wadt, W. R. *J. Chem. Phys.* **1985**, *82*, 299−310.
(34) Hagen, K.; Hedberg, L.; Hedberg, K. *J. Phys. Chem.* **1982**, *86*, 117−121.
(35) Rocha, W. R.; De Almeida, W. B. *J. Comput. Chem.* **1997**, *18*, 254−259.
(36) Anet, F. A. L.; Kozerski, L. *J. Am. Chem. Soc.* **1973**, *95*, 3407−3408.
(37) Ermer, O. *J. Am. Chem. Soc.* **1976**, *98*, 3964−3970.
(38) Pattawong, O.; Salih, M. Q.; Rosson, N. T.; Beaudry, C. M.; Cheong, P. H.-Y. *Org. Biomol. Chem.* **2014**, *12*, 3303−3309.
(39) Lunazzi, L.; Mancinelli, M.; Mazzanti, A. *J. Org. Chem.* **2008**, *73*, 5354−5359.
(40) Example structures with CCDC codes: JAMJOW and TUQWOS.
(41) Cram, D. J.; Choi, H. J.; Bryant, J. A.; Knobler, C. B. *J. Am. Chem. Soc.* **1992**, *114*, 7748−7765.
(42) Hooley, R. J.; Van Anda, H. J.; Rebek, J. *J. Am. Chem. Soc.* **2007**, *129*, 13464−13473.
(43) Fiedler, D.; Bergman, R. G.; Raymond, K. N. *Angew. Chem., Int. Ed.* **2006**, *45*, 745−748.
(44) Nakamura, I.; Shi, A. C. *Phys. Rev. E* **2009**, *80*, 021112.
(45) Kang, J. M.; Rebek, J. *Nature* **1996**, *382*, 239−241.
(46) Inclusion complexes $\mathbf{4}^{+}\subset\mathbf{1}$ and $\mathbf{5}^{+}\subset\mathbf{1}$ were found to be incompetent catalysts in the isomerization reaction of allylic alcohols to ketones.

NOTE ADDED AFTER ASAP PUBLICATION

This paper was published on February 9, 2016. The Acknowledgment has been updated and a link to supporting data has been added. The revised version was re-posted on February 24, 2016.

DOI: 10.1021/jacs.5b12646
J. Am. Chem. Soc. 2016, 138, 2273−2279